Characteristics of foreshock subsolar compressive structures

N. Xirogiannopoulou[1], O. Goncharov[1], J. Šafránková[1], and Z. Němeček[1]

[1]Faculty of Mathematics and Physics, Charles University, Prague, Czech Republic

Key Points:

- Both paramagnetic and diamagnetic plasmoids exist in the foreshock.
- The occurrence rate of the structures increases on highly decelerated solar wind in the foreshock.
- Velocity is deflected from that in the surrounding foreshock inside the SLAMS and mixed structures, but not inside the plasmoids.

Corresponding author: N. Xirogiannopoulou, `=email address=`

Abstract

The turbulent foreshock region upstream of the quasi-parallel bow shock is dominated by waves and reflected particles that interact with each other and create a large number of different foreshock transients. The structures with the enhanced magnetic field (Short Large Amplitude Magnetic Structures, SLAMS) and density spikes named plasmoids are frequently observed. They are one of the suggested sources of transient flux enhancements (TFE) or jets in the magnetosheath. Using measurements of the Magnetospheric Multiscale Spacecraft (MMS) and OMNI solar wind database between the 2015 and 2018 years, we have found that there is a category of events exhibiting both magnetic field and density enhancements simultaneously and we introduce the term "mixed structures" for them. Consequently, we divided our set of observations into three groups of events and present their comparative statistical analysis in the subsolar foreshock. Based on our results and previous research, we discuss the properties, possible origin and occurrence rates these events under different upstream conditions and their possible relation to the jet and plasmoid formation in the magnetosheath.

Plain Language Summary

The solar wind is a plasma stream of charged particles that expands outward from the solar corona. The solar wind on its path first encounters the bow shock, whose structure and properties depend strongly on the angle between the interplanetary magnetic field (IMF) and the shock normal, $\theta \mathrm{B}_n$. Most of the foreshock phenomena, which are the main subjects of this study, are observed for $\theta \mathrm{B}_n < 45^o$, i.e., upstream the quasi-parallel bow shock. The transients like ULF waves, the Short Large Amplitude Magnetic Structures (SLAMS), plasmoids, magnetic holes, etc. are created by interaction of the incoming solar wind and ions reflected from the bow shock. In this paper, we use Magnetospheric Multiscale (MMS) Mission data inside the foreshock and solar wind OMNI database for a statistical study of the properties of these compressive foreshock structures. We show differences between the morphology of the magnetic field, the temperature anisotropy and the occurrence rate of the structures and discuss possible implications for magnetosheath jets.

1 Introduction

Bow shocks appear upstream of both planets and comets. When the supersonic solar wind passes through the bow shock, it is slowed down to subsonic speeds and forms the magnetosheath, which is filled hotter and denser plasma than in the solar wind. The interplanetary magnetic field (IMF) divides the Earth's bow shock region roughly into two areas according to the angle between the bow shock normal and IMF ($\theta \mathrm{B}_n$). If this angle is larger (smaller) than 45°, the shock is called quasi-perpendicular (quasi-parallel). The magnetosheath behind the quasi-parallel bow shock is more turbulent (e.g., Dimmock et al. (2014); Gutynska et al. (2015)) than in the quasi-perpendicular magnetosheath. In recent years, one of the most important avenues in magnetosheath research has been the study of magnetosheath (MSH) jets (e.g., Plaschke et al. (2018)). The MSH jets are significant transient enhancements of the dynamic pressure, which may locally affect the magnetopause. Such structures have been studied under several different names: "transient flux enhancements" (Němeček et al., 1998), "super-fast plasma streams" (Savin et al., 2012), "supermagnetosonic subsolar magnetosheath jets" (Hietala & Plaschke, 2013), "magnetosheath dynamic pressure enhancements" (Archer & Horbury, 2013), "high-speed jets (HSJ)" (Plaschke et al., 2013), "transient density enhancements" (Gutynska et al., 2015), etc. In this paper, we call the structures described in these and related papers "MSH jets."

Karlsson et al. (2012) investigated structures with significant enhancements in the magnetosheath density (an increase of 50% above the mean level) and called them "plas-

moids". Following the Karlsson et al. (2012, 2015) terminology, plasmoids in the magnetosheath can be classified according to their speed and magnetic field variations. The plasmoids convected with the background magnetosheath flow are called "embedded plasmoids" and structures with simultaneous increase of the flow velocity exceeding 10% are called "fast plasmoids". The plasmoids that are associated with a simultaneous decrease in the magnetic field strength are called "diamagnetic" and those associated with an increase in the magnetic field strength are named "paramagnetic". Karlsson et al. (2012) have studied paramagnetic (both embedded and fast) plasmoids in the magnetosheath and considered them as a subset of MSH jets. However, the generation mechanism for MSH jets is still under debate but generally it is suggested that their origin would be related to the interactions between the foreshock structures and bow shock.

At the quasi-parallel shock, solar wind particles flowing toward the bow shock (BS hereafter) can be reflected and stream back upstream along the IMF, forming a foreshock. The turbulent foreshock is occupied by various instabilities, waves and structures, such as compressed ULF waves that grow into Short Large Amplitude Magnetic Structures (SLAMS), hot flow anomalies (HFA), shocklets, cavitons, foreshock bubbles, magnetic holes, plasmoids and many others.

SLAMS are large amplitude magnetic pulsations upstream the quasi-parallel BS (Thomsen et al., 1990; Schwartz & Burgess, 1991; Schwartz et al., 1992), created as a result of the evolution of the compressive ULF waves and their interaction with ion density gradients (Scholer et al., 2003). Their main characteristics are the enhancement of the magnetic field strength inside the structure by a factor of at least 2 compared to their surroundings with a typical duration of 10 s (Schwartz & Burgess, 1991; Schwartz et al., 1992). SLAMS, along with other foreshock structures, are carried towards the BS, forming an extended transition region that contributes to the BS reformation and rippling (e.g., Schwartz and Burgess (1991); Hietala and Plaschke (2013); Plaschke et al. (2013)).

Using a global hybrid-Vlasov simulation, Vlasiator, Palmroth et al. (2018) found that the MHS jets originate due to the interaction of the BS with a high-dynamic-pressure structure that reproduces observational features associated with SLAMS propagating through the magnetosheath. Based on the Vlasiator simulations, Suni et al. (2021) documented that up to 75% of MSH jets are caused by foreshock compressive structures impacting the BS. These compressive structures meet both plasmoids and SLAMS conditions for their formation. On the contrary, Archer et al. (2012) found SLAMS unlikely to be associated with MSH jets. In parallel, Karlsson et al. (2012) linked the origin of the magnetosheath paramagnetic plasmoids to low-amplitude SLAMS. Later, Karlsson et al. (2015) proposed that the magnetosheath diamagnetic, embedded structures may originate in the pristine solar wind.

As numerous previous studies reported that foreshock plasma transients can be formed in the solar wind or foreshock, penetrate through the BS to the magnetosheath and generate MSH jets, we perform a statistical analysis that focuses on the structures observed by the MMS spacecraft in the foreshock region. We concentrate on SLAMS and plasmoids and introduce a new category of transients that meet the criteria for identification of both these structures and call them mixed structures. We study the properties, evolution, and occurrence rates of these three types of structures with the motivation to consider them as possible upstream drivers of their magnetosheath counterparts. In Section 2, we introduce our data sets and argue why we divided them into three sets. In Section 3, we present the occurrence rate of the structures as a function of parameters as observed in both the pristine solar wind and solar wind modified in the foreshock. Section 4 includes discussion of the differences between the classes of structures. Finally, in Section 5 we summarize our findings and make suggestions for future works.

2 Data & Observations

The study is based on data collected from the Magnetospheric Multiscale Spacecraft (MMS) mission (Burch et al., 2016) and solar wind data from the OMNI database

Table 1. Summary of Definitions and Selection Criteria

Denomination	Selection Criterion	Reference	Subsolar
Plasmoids	$N_i \geq 1.5N_o$ & $B \leq 2B_o$	This work	497
SLAMS	$N_i \leq 1.5N_o$ & $B \geq 2B_o$	This work	429
Mixed Structures	$N_i \geq 1.5N_o$ & $B \geq 2B_o$	This work	515
"original" Plasmoids (K12)	$N_i \geq 1.5N_o$	Karlsson et al. (2012)	670
"original" SLAMS (S92)	$B \geq 2B_o$	Schwartz & Burgess (1991)	771

(King & Papitashvili, 2005) between 2015 and 2018. We have visually selected the foreshock regions using the ion energy spectra in MMS Quicklook static plots, confirmed the spacecraft location upstream the Farris and Russell (1994) BS model and selected the observations in the subsolar region (the distance from the X_{GSE} axis is lower than 10 R_E). We use a fast survey mode resolution of the magnetic field (16 Hz) and plasma (4.5 s/sample) measurements (Russell et al., 2016; Pollock et al., 2018). Note that all observations are presented in Geocentric Solar Ecliptic (GSE) coordinates.

For the plasmoid detection, we modified the magnetosheath Karlsson et al. (2012) (K12 hereafter) criterion of an at least 50% of the electron density in a 500 s average window and applied it to the foreshock intervals. We used the increase more than 50% of the ion density, N_i, above the ambient ion density N_o ($N_i > 1.5\ N_o$), computed using a 10-minute running average window. We assume plasma quasi-neutrality, $N_e \sim N_i$ and used N_i instead of the originally applied N_e because the ions carry higher energy. We also checked the electron density and 5-minute running average window, and found nearly perfect overlap with our ion plasmoid identification.

The SLAMS events have been retrieved from the Foghammar Nömtak (2020) list of automatically detected SLAMS in all regions visited by MMS. Their identification is based on the Schwartz et al. (1992) (S92 hereafter) criterion, i.e., an increase of the magnetic field magnitude B inside the structure at least two times above the mean magnetic field strength, B_o ($B \geq 2B_o$). We reduced the set of SLAMS to only cases that cover the time intervals of our selected foreshock and excluded questionable cases by an additional visual inspection.

Criteria used in previous studies and in this paper are summarized in Table 1. Note that our plasmoid definition essentially includes both the diamagnetic and paramagnetic structures that cannot be classified as SLAMS. In addition, we introduce "mixed structures" meeting both K12 and S92 criteria.

Figure 1 shows typical examples of a plasmoid (left), a SLAMS (middle) and a mixed structure (right) observed by MMS1. As the separation among the MMS spacecraft is much smaller than the typical scale sizes of structures, we use data from MMS1 only. Since the foreshock is a highly turbulent region, the magnetic field oscillates as it can be seen in panels 1a, e,i, where the black dashed line stands for the SLAMS threshold. The plasma variations, such as the dynamic pressure, the temperature anisotropy and the ion density are demonstrated in panels 1b-d,f-h,j-l, respectively, the black dashed line in panels 1d,h,l represents the plasmoid threshold. The thresholds are calculated in a 10-minute background frame. The colored vertical boxes set the limits of the structures as indicated by our criteria.

It can be seen that the change of the density does not imply a peak in the magnetic field (panels a, d) and vice versa (panels e, h). In all structures, the dynamic pressure is in perfect correlation with the density profile (panels 1b, d, 1f, h and 1j, l), implying that there is a negligible change of the velocity inside them. A comparison of magnetic field panels reveals that the variations inside the plasmoid (panel 1a) are notably smoother than inside SLAMS (panel 1e) and mixed structure (panel 1i) exhibits an intermediate behavior. The magnetic field of the plasmoids exhibits a rotation towards the end and after the structures. This rotation coincides with a drop in the dynamic pres-

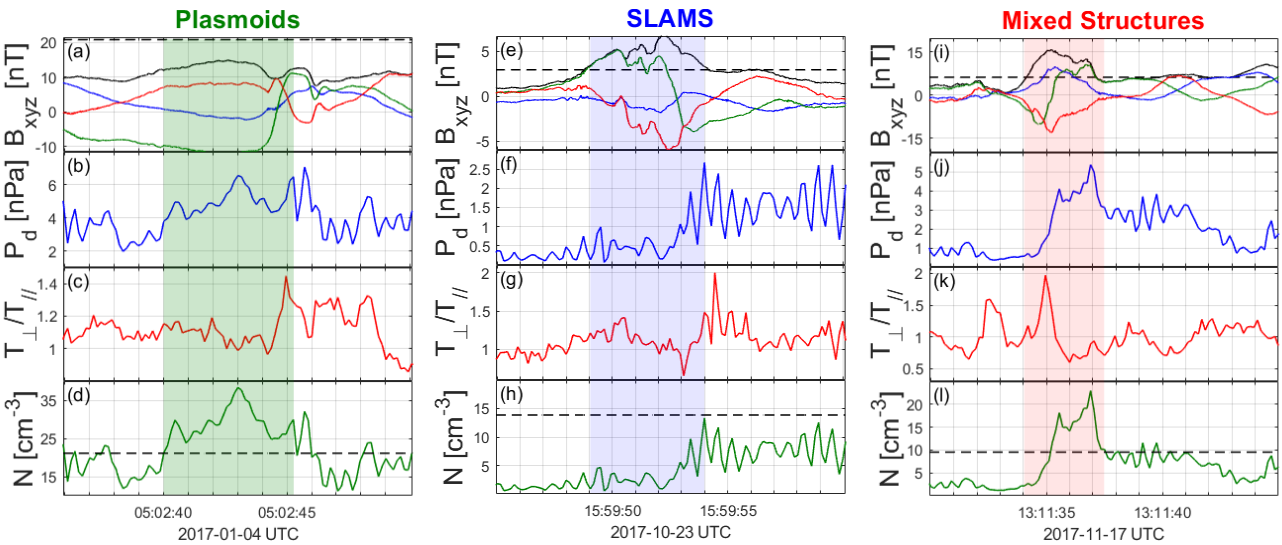

Figure 1. Examples of foreshock plasmoids (a-d), SLAMS (e-h) and mixed structures (i-l) by MMS1 in burst mode. From top to bottom: (a,e,i) magnetic field, (|B|-black; B_x-blue; B_y-green; B_z-red); (b,f,j) dynamic pressure; (c,g,k) temperature anisotropy $T_\perp/T_{//}$; (d,h,l) ion density. The black dashed lines in panels (a,e,i) and (d,h,l) represent threshold values for SLAMS and plasmoids detection respectively.

sure and density and a peak in the perpendicular temperature and it suggests their connection with magnetic field discontinuities created by the nonlinear interaction of foreshock waves. On the contrary, the SLAMS magnetic field rotates inside the structure. Oppositely to plasmoids, this rotation is associated with perpendicular cooling and trail of peaks in the dynamic pressure and density. Last but not least, the magnetic field in the mixed structures passes the threshold earlier than the density. By the time that B_y rotates inside, we detect the sudden increase in the density and dynamic pressure, followed by intense perpendicular cooling. A brief view on the basic characteristics of the structures indicates some similarities (ex., little or no change of the velocity) but also some differences between them (ex., the correlation of the density and magnetic field in structures).

The upstream parametres can affect the formation of the foreshock, especially the IMF orientation. In this paper, we present a statistical analysis, according to the location in the X-R_{GSE} plane, where $R_{GSE} = (Y^2_{GSE} + Z^2_{GSE})^{1/2}$. To analyze the influence of the ambient (background) conditions, each event was completed with median values of density, velocity and magnetic field computed over 3-minute intervals around the structures. Based on these parameters, were estimated the distances to the BS model (Farris & Russell, 1994), along the Sun-Earth line. The upstream solar wind parameters were obtained from the high resolution 1-min OMNI data propagated to the bow shock nose (`https://omniweb.gsfc.nasa.gov/ow_min.html`). To minimize it and decrease the influence of the uncertainty of the solar wind propagation from the L1 point to the BS, all upstream solar wind parameters were averaged over 2 minutes before and after the registration of the structures.

Figure 2 shows relative changes of the magnetic field magnitude (B_{inside}/B_{before}) and ion density (N_{inside}/N_{before}) over the structures. One can note that our plasmoids are mostly paramagnetic and the diamagnetic plasmoids represent only 4% of the orig-

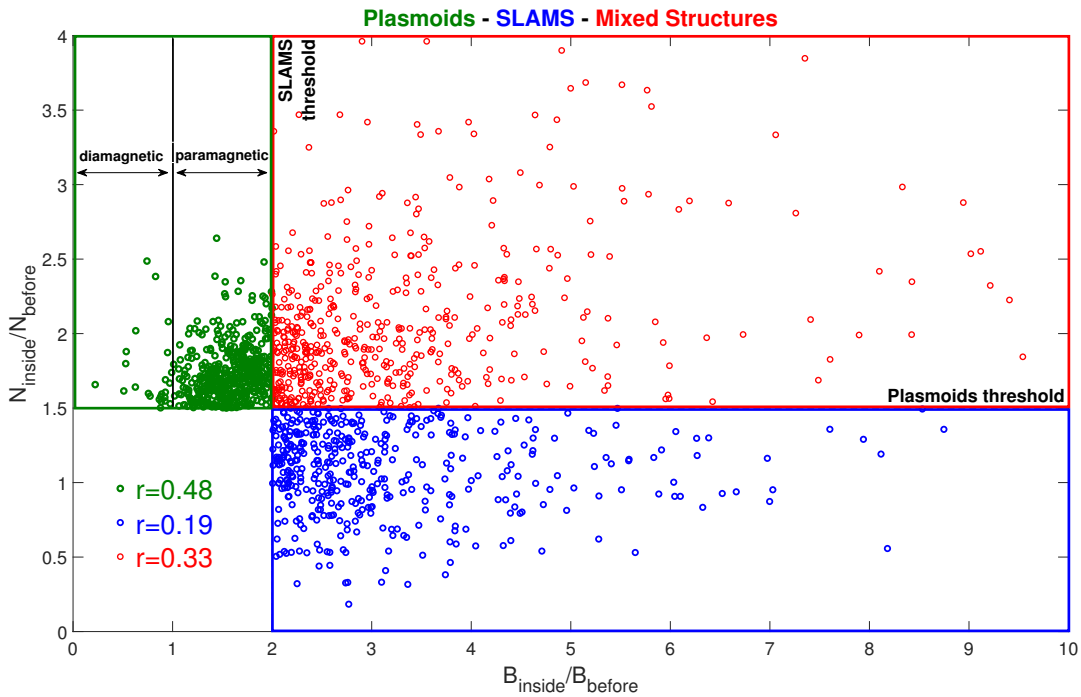

Figure 2. Relative change of magnetic field magnitude (x-axis) and density (y-axis) prior to and inside the plasmoids (green), the SLAMS (blue) and the mixed structures (red), accompanied with the Spearmann correlation coefficient, r.

inal set. This result is unexpected because, according to Karlsson et al. (2012), only diamagnetic plasmoids are present upstream the BS (in the pristine solar wind) while paramagnetic signatures are connected with SLAMS. The authors suggested that the magnetosheath paramagnetic plasmoids are probably generated at the BS but it cannot be applied on foreshock plasmoids. Karlsson et al. (2015) show some examples of SW plasmoids with anti-correlation of B and N. As far as the SLAMS are concerned, older studies suggest that the density inside SLAMS should be in phase with the magnetic field magnitude (Behlke et al., 2003). Most recent studies, however, show the cases with out of phase increases of the density and magnetic field, either due to shock reformation (Turner et al., 2021) or due to non-linear gyro trapping (Chen et al., 2018). The Pearson correlation coefficient between the magnetic field and density equals to 0.144 in our structures and it means little or no connection between these quantities.

3 Statistical Study

Each event was completed with median values of the density, velocity and magnetic field computed over 3-minute intervals around the structures. Based on these parameters, we estimated the distances to the BS model Farris and Russell (1994), along the X direction. The upstream solar wind parameters were obtained from the 1-min OMNI data (`https://omniweb.gsfc.nasa.gov/ow_min.html`). To decrease the influence of the uncertainty of the solar wind propagation from the L1 point to BS, all upstream solar wind parameters were averaged over 4 minutes centered to the time of the structure registration.

Figure 3 shows the number of structures created per hour for plasmoids (green), SLAMS (blue) and mixed structures (red) as a function of OMNI upstream parameters.

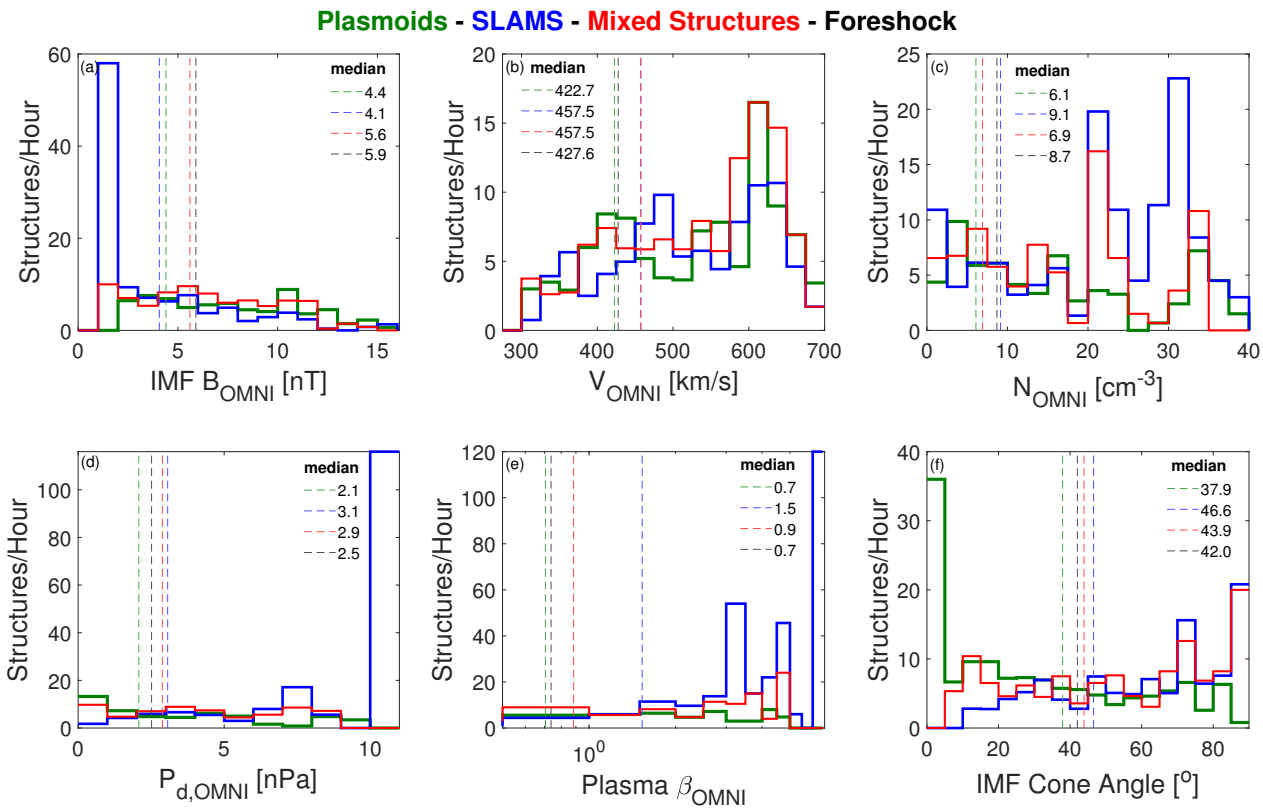

Figure 3. (a-f) Occurrence rate of plasmoids (green), SLAMS (blue) and mixed structures (red), as a function of the upstream parametres. (a) IMF magnitude; (b) solar wind speed; (c) solar wind density; (d) solar wind dynamic pressure; (e) plasma β; (f) IMF cone angle.

The color dashed lines show medians for a particular structure, the black dashed line stands for median of this parameter in the foreshock. The differences between median values are generally very small with exception of the plasma β computed as ratio of proton and magnetic pressures (Figure 3e). Whereas the median β for our foreshock intervals is about 0.7 and similar values (0.7 and 0.9, respectively) were found for plasmoids and mixed structures, it is about 1.5 for SLAMS. This is consistent with a decreasing trend in Figure 3a showing the dependence of the occurrence rate on B_{OMNI} and panel 3c that demonstrates increase of the SLAMS occurrence rate with the upstream density. A common feature of all structures is an increasing occurrence rate with increasing V_{OMNI}. We think that the decrease observed for velocities above 650 km/s is only apparent and connected with a very small number of observations under such conditions and the same is probably true for the peak of plasmoid occurrence rate in the bin of lowest IMF cone angle (Fig 3f). It should be noted that the BS in the investigated region would be quasi-perpendicular for the IMF cone angle larger than 75° and thus there would be no foreshock for these cone angles. Since our identification of foreshock intervals is based on the presence of energetic particles, an occurrence of the foreshock for these cone angles is probably caused by uncertainty of OMNI IMF direction determination. Consequently, the increase of the occurrence rate of SLAMS and mixed structures at large cone angles is artificial.

The investigated structures are excited in the foreshock and they are blown down with the solar wind flow and they can grow or decay under some conditions. Moreover, it was shown that the mean magnetic field and plasma parameters are modified in the foreshock. For this reason, 2D histograms, in Figure 4, present the occurrence rates (color bar) of plasmoids (panels 4a-c), SLAMS (panels 4d-f) and mixed structures (panels 4g-i) as a function of distance to the BS for the changes of the magnetic field magnitude B, velocity V, and density, N in the solar wind and in foreshock. The values of B, V and N in the foreshock (sub-scripted "F") are averages of the MMS foreshock measurements (on the interval of 5 minutes) and the solar wind values (sub-scripted "OMNI") are OMNI data averaged over the same interval. A distance from the BS was computed as the distance of the spacecraft according to the Farris and Russell (1994) model along the X_{GSE} direction (approximately the solar wind direction) using local MMS parameters measured prior to the structure.

We would like to note that the foreshock values vary in broad ranges around corresponding upstream values; the ratios vary from 0.5 to 2 for the magnetic field strength and plasma density and between 0.6 and 1.2 for the velocity. Although the values used for computation of these ratios become from the different spacecraft and upstream parameters are propagated from the L1 point, these ranges are surprising. Urbář et al. (2019) studied modification of the solar wind velocity in the foreshock using similar technique and THEMIS/ARTEMIS data and found up to 5% deceleration in front of the BS. We are not aware of similar studies of the density or magnetic field strength but the ranges following from the figure are surprisingly broad. Although the structures are preferentially observed in fast solar wind (Figure Figure 3), their occurrence rate increases with deceleration of the solar wind in the foreshock and this trend is more pronounced for magnetic (SLAMS and mixed) structures. This trend is compatible with preference for a compressed (N_F/N_{OMNI} >1 and/or B_F/B_{OMNI} <1) foreshock. The only exclusion are SLAMS, they can be observed either for B_F/B_{OMNI} >1 or for B_F/B_{OMNI} <1. All panels indicate a clear increase of the occurrence rate toward the BS.

4 Superposed epoch analysis

Figure 5 shows a superposed epoch analysis of the angles between the velocity and magnetic field vectors and the X_{GSE} axis (cone angles) and the temperature anisotropy on one minute around plasmoids (a-c), SLAMS (d-f) and mixed structures (g-j). The color lines show variations of the median values, the gray lines around are the first and the third quartiles. The fact that the quartiles exhibit the same trends as medians ensures that the median profiles can be taken as the representatives of particular structures. The

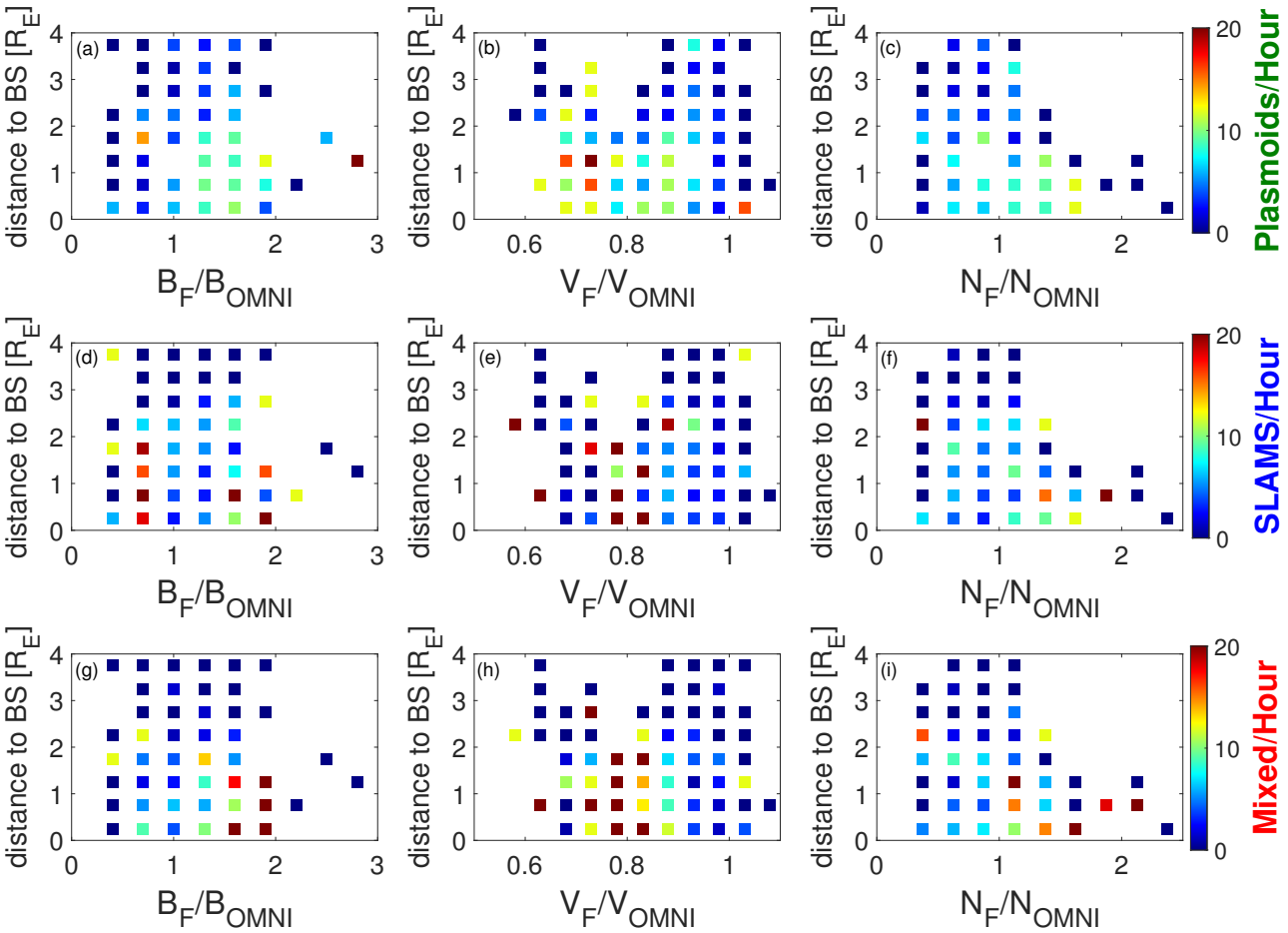

Figure 4. 2D histograms of occurrence rate of plasmoids (a-c), SLAMS (d-f) and mixed structures (g-i) as a function of modification of the magnetic field magnitude B_F/B_{OMNI} (a,d,g), the velocity V_F/V_{OMNI} (b,e,h) and the density N_F/N_{OMNI} (c,f,i) in the surrounding foreshock and in different distances to the BS.

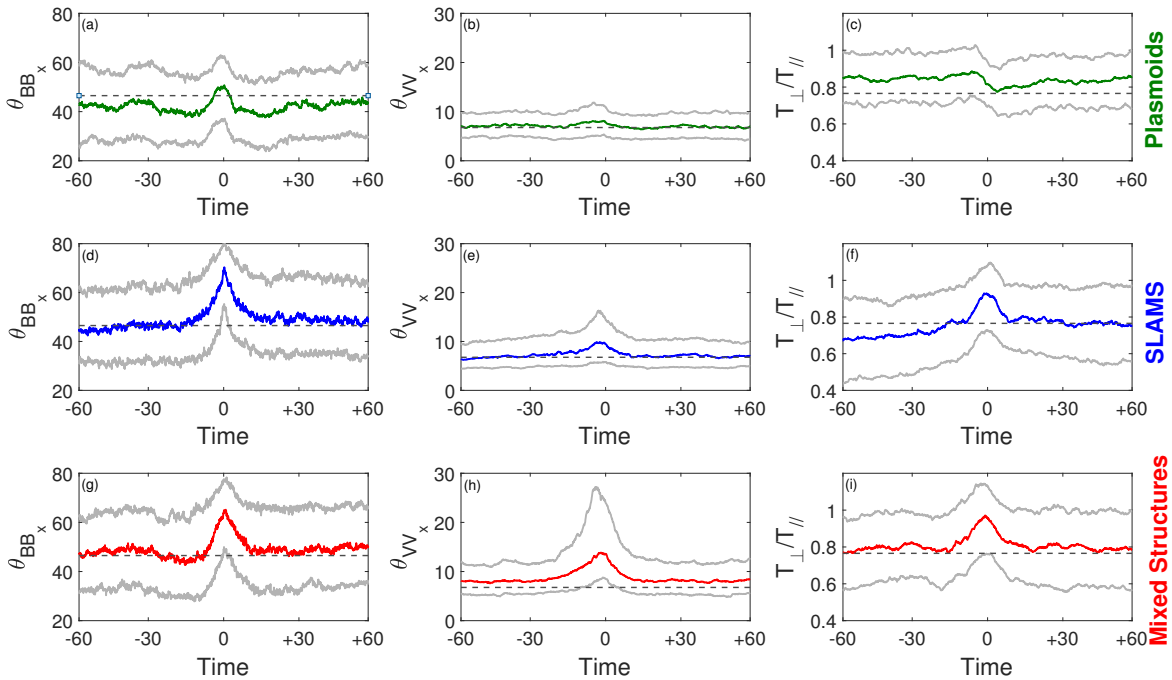

Figure 5. Superposed epoch analysis of the angles between the magnetic field vector θBB_x (a, d, g) and velocity vector θVV_x (b, e, h) and the X_{GSE} axis and the temperature anisotropy $T_\perp/T_{//}$ (c, f, i) of plasmoids (a-c), SLAMS (d-f) and mixed structures (g-i). Each structure's peak is positioned in time zero. Color lines are the medians and grey lines represent the first (bottom line) and the third (top lines) quartiles.

dashed horizontal lines are median values of each parameter calculated for our foreshock intervals. We can note that these values almost coincide with the values observed prior to and after structures. It is hard to say whether the lower magnetic field cone angle (panel 5a) or lower temperature anisotropy (panel 5c) around plasmoids is significant or whether is it connected with a relatively small number of cases. On the other hand, all parameters inside the structures exhibit significant deviations from foreshock median values. The magnetic field turns to larger cone angles and the same is true for velocity. This effect is surprising especially for plasmoids because one would expect that they would tend to keep the original flow direction or to move more radially. The suggested origin of studied intermittent structures is nonlinear interaction of foreshock waves and enlarged temperature anisotropy in front of SLAMS seems to confirm this suggestion but the nearly isotropic temperature inside SLAMS and mixed structures contradict to it. Plasmoids are created in regions with a larger anisotropy than mixed structures or SLAMS and we observe perpendicular cooling inside them. It agrees with the paramagnetic plasmoids in the magnetosheath but not in the solar wind (Karlsson et al., 2012).

5 Discussion

We present a statistical study of the 1441 foreshock structures divided into three categories (497 plasmoids, 429 SLAMS and 515 mixed structures) in wide ranges of distances from the BS and upstream parameters. In general, many criteria can be applied

to different parameters (density, magnetic field magnitude, dynamic pressure along the X_{GSE} axis etc.) in the turbulent foreshock and it is still challenging to define all structures and transients. We slightly modified the observational criteria used in past for plasmoids (Karlsson et al., 2012) and for SLAMS (Schwartz et al., 1992) and introduced the category of mixed structures that meets both criteria. The reason for distinguishing the structures that possess characteristics of both SLAMS and plasmoids is that we expect that the interaction of such structures with the BS can results in major disturbances in the magnetosheath and thus, they are best candidates for a creation of MSH jets. Nevertheless, it should be noted that a selection of the structures into categories is rather artificial because Figure 1 shows that there are no distinct groups in the magnetic field-density space but rather a smooth transition from one to other category is observed. We thus cannot exclude the transition of a particular structure from one to another category in course of its propagation toward the BS.

Scholer et al. (2003) proposed that SLAMS are generated by ULF wave steepening. Karlsson et al. (2015) suggested that diamagnetic plasmoids can be generated in the solar wind, but paramagnetic cases are most likely created in the BS ripples and thus they would be observed in the BS vicinity only. However, the exact origin of plasmoids and SLAMS in the foreshock is still under investigations. Therefore, we attempted to determine the factors that influence the structure formation using two different environments, the pristine solar wind (Figure 3) and the foreshock (Figure 4). All structures are observed in the whole range of upstream conditions but their occurrence rate increases with the solar wind speed. SLAMS are created preferentially in the low IMF and high density (i.e., high beta) solar wind, other structures do not exhibit any clear preference for particular upstream conditions. However, the foreshock processes modify mean upstream parameters and thus Figure 4 demonstrates the occurrence rates of different structures as a function of this modification. First of all, we should note that this modification is very significant (see Figure 4) and it suggests that our relatively short structures are a part of or are created within much larger structures with duration exceeding 5 minutes (duration of intervals for averaging). Such structures are characterized by a significant solar wind deceleration (20% or more) and enhanced density and magnetic field strength. However, SLAMS are also frequently observed in the regions of magnetic field depletion. These findings connect investigated intermitted foreshock structures with overall foreshock structure. The superposed epoch analysis (Figure 5) reveals small systematic changes of the velocity and magnetic field direction inside SLAMS and mixed structures. The velocity inside these structures turns out of the radial direction and it means that the structures help in preconditioning of the solar wind prior to it enters the magnetosheath (Sibeck et al., 2001). The mean magnetic field around the structures follows the Parker spiral orientation but this orientation tends to be more perpendicular to the Sun-Earth line within structures. This trend is consistent with the velocity direction change.

The studies of MSH jets conducted so far indicate that foreshock structures, especially SLAMS, combined with the BS ripples are responsible for the creation of the majority of them (e.g., Hietala et al. (2012); Hietala and Plaschke (2013); Karlsson et al. (2015)). Some studies (Karlsson et al., 2012, 2015) suggest that foreshock plasma transients can penetrate through the BS to magnetosheath and generate MSH jets. Using ion-kinetic Vlasiator simulations, Suni et al. (2021) show that MSH jets are related to foreshock compressive structures. The relation between foreshock structures and MSH jets is not straightforward because Blanco-Cano et al. (2023) discusses the jets observed in the magnetosheath behind the quasi-perpendicular BS that have local sources and do not depend on upstream structures. Moreover, the jets in the magnetosheath are often mixed with plasmoids embedded in the flow that are created locally by reconnection in the highly turbulent environment just behind the BS (Luis Preisser et al., 2020).

Since the direct experimental evidence of a connection of foreshock structures with the MSH jets is difficult if not impossible, let us compare the dependence of the occurrence rates of foreshock structures determined in our study with the rates published for MSH jets. Early study by Plaschke et al. (2013) suggests the IMF cone angle as the most

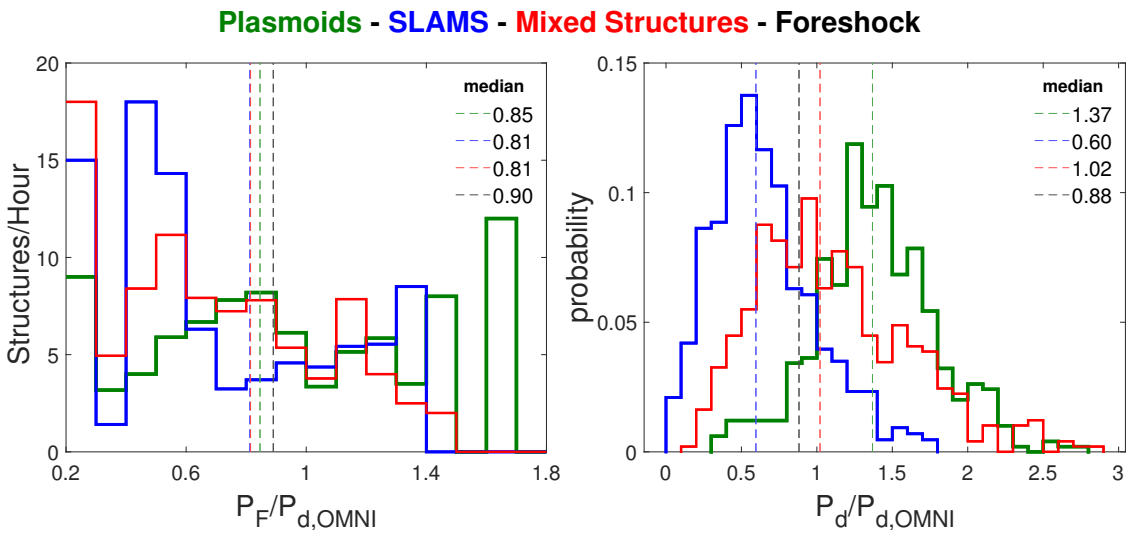

Figure 6. (a) Occurrence rate of the structures as a function of the modification of the dynamic pressure inside the surrounding foreshock; (b) Histogram of peak values of the dynamic pressure inside the structures normalized to the solar wind dynamic pressure for all structure types.

important controlling factor for MSH jet creation and this factor is emphasized also in other studies (Goncharov et al., 2020; LaMoury et al., 2021; Koller et al., 2023) but our results (Figure 3f) show a weak or no dependence of the occurrence rates of foreshock structures on the cone angle. LaMoury et al. (2021) and Koller et al. (2023) show that a low IMF magnitude plays an important role in jet creation and it is consistent with trends found for all analyzed foreshock structures. On the other hand, high IMF strength increases the probability that the jets reach the magnetopause (Goncharov et al., 2020; LaMoury et al., 2021; Koller et al., 2023) argue that jet occurrence rate increases with the upstream velocity that is consistent with our observations for all foreshock structures. Our analysis reveals increased SLAMS and mixed structure the occurrence rates for high beta that agree with conditions for jets in Goncharov et al. (2020) but the low density condition suggested by LaMoury et al. (2021) is held only for foreshock plasmoids because the highest occurrence rates of SLAMS and mixed structures were observed for densities exceeding 20cm^{-3}. If we combine all above comparisons we can conclude that foreshock plasmoids are a most probable candidate for the MSH jet seeds because SLAMS and mixed structures are more frequently observed in the dense solar wind.

Since the most important characteristics of MSH jets is the dynamic pressure, Figure 6 presents a relation of the dynamic pressure around (panel 6a) and inside (panel 6b) to the OMNI pressure. Figure 6a shows that the structures characterized by the magnetic field enhancement (SLAMS and mixed structures) are more frequently observed in the regions of the depressed dynamic pressure whereas plasmoids prefer the enhanced pressure. These preferences are consistent with already discussed modification of foreshock parameters. The largest enhancements of the dynamic pressure are found in plasmoids (median factor of 1.37) while SLAMS exhibits a pressure decrease (median factor of 0.60). If we compare this finding with the deviation of the velocity direction (Figure 5) that is lowest for plasmoids, it supports the above hypothesis on the plasmoids (and maybe mixed structures) being the most probable source of MSH jets.

6 Conclusion

Our statistical study of compressive structures in the subsolar foreshock divides these structures into three categories (plasmoids, SLAMS and mixed structures) with motivation to find conditions favorable for development of a particular category. Our conclusions can be summarized as it follows.

1. There is no clear separation between the structure categories in the N_{inside}/N_{before} – B_{inside}/B_{before} parameter space, rather continuous transition is observed (Figure 2).
2. Both paramagnetic and diamagnetic plasmoids exist in the foreshock, but paramagnetic structures are dominant (Figure 2).
3. Occurrence rate of all structures rises with the solar wind speed (Figure 3).
4. SLAMS and mixed structures are more frequently observed in the less magnetized and denser solar wind (i.e., higher plasma β). Plasmoids are observed under lower cone angles (Figure 3).
5. All structures are predominantly observed in the foreshock regions where the upstream magnetic field and plasma parameters are strongly modified - the velocity is decreased by a factor of 0.7-0.8, density and magnetic field are enhanced by a factor of ~ 1.5. The only exceptions are SLAMS that can be also frequently observed in regions of the depressed magnetic field (Figure 4).
6. Occurrence rates of all structures decrease with distance from the BS (Figure 4).
7. SLAMS and mixed structures are characterized by increase of the perpendicular temperature but a slight perpendicular cooling is observed inside plasmoids (Figure 5).
8. All structures are characterized by a deflection of the magnetic field and velocity direction from those in the surrounding foreshock; the deflection in plasmoids is the lowest one (Figure 5).
9. A great majority of plasmoids and about a half of mixed structures exhibit the enhancement of the dynamic pressure with respect to the upstream value. The dynamic pressure inside SLAMS is, as a rule, lower than the upstream value (Figure 6).

The structures under study are relatively small, typical dimensions are of the order of thousands of km but they are a part of much larger structures (point 5). We suggest that the modification/reformation of the bow shock that results in formation of MSH jets is probably caused by these large structures. Nevertheless, the change of velocity direction and dynamic pressure inside the analyzed structures (points 8 and 9) suggest that the interaction of the structures carrying plasmoids or mixed structures would result to MSH jets with a larger probability. On the other hand, a rotation of the magnetic field inside SLAMS locally changes the BS geometry and it can lead to the creation of a dip on its surface and formation of the jet by the mechanisms suggested by (Hietala & Plaschke, 2013) or Raptis et al. (2022). However, in-depth analysis of plasmoids, SLAMS and mixed structures, their generation and connection to the MSH jets are required and will be carried out in the near future.

Data Availability Statement

All data is available through `https://lasp.colorado.edu/mms/sdc/public/` and `https://omniweb.gsfc.nasa.gov/`.

Acknowledgments

The present work was supported by the Czech Science Foundation under Contract 21-26463S. We thank the MMS Science Data Center and all the MMS teams, especially the

magnetic field and the ion teams, for producing high-quality data. We also acknowledge NASA's National Space Science Data Center and Space Physics Data Facility.

References

Archer, M. O., & Horbury, T. S. (2013). Magnetosheath dynamic pressure enhancements: occurrence and typical properties. *Annales Geophysicae*, *31*(2), 319–331. Retrieved from `https://angeo.copernicus.org/articles/31/319/2013/` doi: 10.5194/angeo-31-319-2013

Archer, M. O., Horbury, T. S., & Eastwood, J. P. (2012). Magnetosheath pressure pulses: Generation downstream of the bow shock from solar wind discontinuities. *Journal of Geophysical Research: Space Physics*, *117*(A5). Retrieved from `https://agupubs.onlinelibrary.wiley.com/doi/abs/10.1029/2011JA017468` doi: https://doi.org/10.1029/2011JA017468

Behlke, R., André, M., Buchert, S. C., Vaivads, A., Eriksson, A. I., Lucek, E. A., & Balogh, A. (2003). Multi-point electric field measurements of short large-amplitude magnetic structures (slams) at the earth's quasi-parallel bow shock. *Geophysical Research Letters*, *30*(4). Retrieved from `https://agupubs.onlinelibrary.wiley.com/doi/abs/10.1029/2002GL015871` doi: https://doi.org/10.1029/2002GL015871

Blanco-Cano, X., Rojas-Castillo, D., Kajdič, P., & Preisser, L. (2023). Jets and mirror mode waves in earth's magnetosheath. *Journal of Geophysical Research: Space Physics*, *128*(7), e2022JA031221. Retrieved from `https://agupubs.onlinelibrary.wiley.com/doi/abs/10.1029/2022JA031221` (e2022JA031221 2022JA031221) doi: https://doi.org/10.1029/2022JA031221

Burch, J. L., Moore, T. E., Torbert, R. B., & Giles, B. L. (2016). Magnetospheric multiscale overview and science objectives. *Space Science Reviews*, *199*, 5-21. doi: https://doi.org/10.1007/s11214-015-0164-9

Chen, L.-J., Wang, S., Wilson, L. B., Schwartz, S., Bessho, N., Moore, T., ... Avanov, L. (2018, May). Electron bulk acceleration and thermalization at earth's quasiperpendicular bow shock. *Phys. Rev. Lett.*, *120*, 225101. Retrieved from `https://link.aps.org/doi/10.1103/PhysRevLett.120.225101` doi: 10.1103/PhysRevLett.120.225101

Dimmock, A. P., Nykyri, K., & Pulkkinen, T. I. (2014). A statistical study of magnetic field fluctuations in the dayside magnetosheath and their dependence on upstream solar wind conditions. *Journal of Geophysical Research: Space Physics*, *119*(8), 6231-6248. Retrieved from `https://agupubs.onlinelibrary.wiley.com/doi/abs/10.1002/2014JA020009` doi: https://doi.org/10.1002/2014JA020009

Farris, M. H., & Russell, C. T. (1994). Determining the standoff distance of the bow shock: Mach number dependence and use of models. *Journal of Geophysical Research: Space Physics*, *99*(A9), 17681-17689. Retrieved from `https://agupubs.onlinelibrary.wiley.com/doi/abs/10.1029/94JA01020` doi: https://doi.org/10.1029/94JA01020

Foghammar Nömtak, C. (2020). Automatic slams detection and magnetospheric classification in mms data. *KTH, School of Electrical Engineering and Computer Science (EECS)*.

Goncharov, O., Gunell, H., Hamrin, M., & Chong, S. (2020). Evolution of high-speed jets and plasmoids downstream of the quasi-perpendicular bow shock. *Journal of Geophysical Research: Space Physics*, *125*(6), e2019JA027667. Retrieved from `https://agupubs.onlinelibrary.wiley.com/doi/abs/10.1029/2019JA027667` (e2019JA027667 2019JA027667) doi: https://doi.org/10.1029/2019JA027667

Gutynska, O., Sibeck, D. G., & Omidi, N. (2015). Magnetosheath plasma structures and their relation to foreshock processes. *Journal of Geophysical*

Research: Space Physics, *120*(9), 7687-7697. Retrieved from https://agupubs.onlinelibrary.wiley.com/doi/abs/10.1002/2014JA020880 doi: https://doi.org/10.1002/2014JA020880

Hietala, H., Partamies, N., Laitinen, T. V., Clausen, L. B. N., Facskó, G., Vaivads, A., ... Lucek, E. A. (2012). Supermagnetosonic subsolar magnetosheath jets and their effects: from the solar wind to the ionospheric convection. *Annales Geophysicae*, *30*(1), 33–48. Retrieved from https://angeo.copernicus.org/articles/30/33/2012/ doi: 10.5194/angeo-30-33-2012

Hietala, H., & Plaschke, F. (2013). On the generation of magnetosheath high–speed jets by bow shock ripples. *Journal of Geophysical Research: Space Physics*, *118*(11), 7237-7245. Retrieved from https://agupubs.onlinelibrary.wiley.com/doi/abs/10.1002/2013JA019172 doi: https://doi.org/10.1002/2013JA019172

Karlsson, T., Brenning, N., Nilsson, H., Trotignon, J.-G., Vallières, X., & Facsko, G. (2012). Localized density enhancements in the magnetosheath: Three-dimensional morphology and possible importance for impulsive penetration. *Journal of Geophysical Research: Space Physics*, *117*(A3). Retrieved from https://agupubs.onlinelibrary.wiley.com/doi/abs/10.1029/2011JA017059 doi: https://doi.org/10.1029/2011JA017059

Karlsson, T., Kullen, A., Liljeblad, E., Brenning, N., Nilsson, H., Gunell, H., & Hamrin, M. (2015). On the origin of magnetosheath plasmoids and their relation to magnetosheath jets. *Journal of Geophysical Research: Space Physics*, *120*(9), 7390-7403. Retrieved from https://agupubs.onlinelibrary.wiley.com/doi/abs/10.1002/2015JA021487 doi: https://doi.org/10.1002/2015JA021487

King, J. H., & Papitashvili, N. E. (2005). Solar wind spatial scales in and comparisons of hourly wind and ace plasma and magnetic field data. *Journal of Geophysical Research: Space Physics*, *110*(A2). Retrieved from https://agupubs.onlinelibrary.wiley.com/doi/abs/10.1029/2004JA010649 doi: https://doi.org/10.1029/2004JA010649

Koller, F., Plaschke, F., Temmer, M., Preisser, L., Roberts, O. W., & Vörös, Z. (2023). Magnetosheath jet formation influenced by parameters in solar wind structures. *Journal of Geophysical Research: Space Physics*, *128*(4), e2023JA031339. Retrieved from https://agupubs.onlinelibrary.wiley.com/doi/abs/10.1029/2023JA031339 (e2023JA031339 2023JA031339) doi: https://doi.org/10.1029/2023JA031339

LaMoury, A. T., Hietala, H., Plaschke, F., Vuorinen, L., & Eastwood, J. P. (2021). Solar wind control of magnetosheath jet formation and propagation to the magnetopause. *Journal of Geophysical Research: Space Physics*, *126*(9), e2021JA029592. Retrieved from https://agupubs.onlinelibrary.wiley.com/doi/abs/10.1029/2021JA029592 (e2021JA029592 2021JA029592) doi: https://doi.org/10.1029/2021JA029592

Luis Preisser, L., Blanco-Cano, X., Kajdič, P., Burgess, D., & Trotta, D. (2020). Magnetosheath jets and plasmoids: Characteristics and formation mechanisms from hybrid simulations. *The Astrophysical Journal Letters*, *900*. doi: https://10.3847/2041-8213/abad2b

Němeček, Z., Šafránková, J., Přech, L., Sibeck, D. G., Kokubun, S., & Mukai, T. (1998). Transient flux enhancements in the magnetosheath. *Geophysical Research Letters*, *25*(8), 1273-1276. Retrieved from https://agupubs.onlinelibrary.wiley.com/doi/abs/10.1029/98GL50873 doi: https://doi.org/10.1029/98GL50873

Palmroth, M., Ganse, U., Pfau-Kempf, Y., Battarbee, M., Turc, L., Brito, T., ... von Alfthan, S. (2018). Vlasov methods in space physics and astrophysics. *Living reviews in computational astrophysics*, *4*(1). doi: https://doi.org/10.1007/s41115-018-0003-2

Plaschke, F., Hietala, H., & Angelopoulos, V. (2013). Anti-sunward high-speed jets in the subsolar magnetosheath. *Annales Geophysicae*, *31*(10), 1877–1889. Retrieved from https://angeo.copernicus.org/articles/31/1877/2013/ doi: 10.5194/angeo-31-1877-2013

Plaschke, F., Hietala, H., Archer, M., Blanco-Cano, X., Kajdič, P., Karlsson, T., ... Sibeck, D. (2018). Jets downstream of collisionless shocks. *Space Science Reviews*, *214*(81). Retrieved from https://rdcu.be/dkFR4 doi: https://doi.org/10.1007/s11214-018-0516-3

Pollock, C., Burch, J., Chasapis, A., Giles, B., Mackler, D., Matthaeus, W., & Russell, C. (2018). Magnetospheric multiscale observations of turbulent magnetic and electron velocity fluctuations in earth's magnetosheath downstream of a quasi-parallel bow shock. *Journal of Atmospheric and Solar-Terrestrial Physics*, *177*, 84-91. Retrieved from https://www.sciencedirect.com/science/article/pii/S1364682617303899 (Dynamics of the Sun-Earth System: Recent Observations and Predictions) doi: https://doi.org/10.1016/j.jastp.2017.12.006

Raptis, S., Karlsson, T., Vaivads, A., Pollock, C., Plaschke, F., Johlander, A., ... Lindqvist, P.-A. (2022). Downstream high-speed plasma jet generation as a direct consequence of shock reformation. *Nature Communications*, *13*. doi: https://doi.org/10.1038/s41467-022-28110-4

Russell, C. T., Anderson, B. J., Baumjohann, W., Bromund, K. R., Dearborn, D., Fischer, D., ... Richter, I. (2016). The magnetospheric multiscale magnetometers. *Space Science Reviews*, *199*, 189–256. doi: https://doi.org/10.1007/s11214-014-0057-3

Savin, S., Amata, E., Zelenyi, L., Lutsenko, V., Safrankova, J., Nemecek, Z., ... Lezhen, L. (2012). Super fast plasma streams as drivers of transient and anomalous magnetospheric dynamics. *Annales Geophysicae*, *30*(1), 1-7. Retrieved from https://angeo.copernicus.org/articles/30/1/2012/ doi: 10.5194/angeo-30-1-2012

Scholer, M., Kucharek, H., & Shinohara, I. (2003). Short large-amplitude magnetic structures and whistler wave precursors in a full-particle quasi-parallel shock simulation. *Journal of Geophysical Research: Space Physics*, *108*(A7). Retrieved from https://agupubs.onlinelibrary.wiley.com/doi/abs/10.1029/2002JA009820 doi: https://doi.org/10.1029/2002JA009820

Schwartz, S. J., & Burgess, D. (1991). Quasi-parallel shocks: A patchwork of three-dimensional structures. *Geophysical Research Letters*, *18*(3), 373-376. Retrieved from https://agupubs.onlinelibrary.wiley.com/doi/abs/10.1029/91GL00138 doi: https://doi.org/10.1029/91GL00138

Schwartz, S. J., Burgess, D., Wilkinson, W. P., Kessel, R. L., Dunlop, M., & Lühr, H. (1992). Observations of short large-amplitude magnetic structures at a quasi-parallel shock. *Journal of Geophysical Research: Space Physics*, *97*(A4), 4209-4227. Retrieved from https://agupubs.onlinelibrary.wiley.com/doi/abs/10.1029/91JA02581 doi: https://doi.org/10.1029/91JA02581

Sibeck, D. G., Decker, R. B., Mitchell, D. G., Lazarus, A. J., Lepping, R. P., & Szabo, A. (2001). Solar wind preconditioning in the flank foreshock: Imp 8 observations. *Journal of Geophysical Research: Space Physics*, *106*(A10), 21675-21688. Retrieved from https://agupubs.onlinelibrary.wiley.com/doi/abs/10.1029/2000JA000417 doi: https://doi.org/10.1029/2000JA000417

Suni, J., Palmroth, M., Turc, L., Battarbee, M., Johlander, A., Tarvus, V., ... Zhou, H. (2021). Connection between foreshock structures and the generation of magnetosheath jets: Vlasiator results. *Geophysical Research Letters*, *48*(20), e2021GL095655. Retrieved from https://agupubs.onlinelibrary.wiley.com/doi/abs/10.1029/2021GL095655 (e2021GL095655 2021GL095655) doi: https://doi.org/10.1029/2021GL095655

Thomsen, M. F., Gosling, J. T., Bame, S. J., & Russell, C. T. (1990). Mag-

netic pulsations at the quasi-parallel shock. *Journal of Geophysical Research: Space Physics*, *95*(A2), 957-966. Retrieved from https://agupubs.onlinelibrary.wiley.com/doi/abs/10.1029/JA095iA02p00957 doi: https://doi.org/10.1029/JA095iA02p00957

Turner, D. L., Wilson, L. B., Goodrich, K. A., Madanian, H., Schwartz, S. J., Liu, T. Z., ... Burch, J. L. (2021, apr). Direct multipoint observations capturing the reformation of a supercritical fast magnetosonic shock. *The Astrophysical Journal Letters*, *911*(2), L31. Retrieved from https://dx.doi.org/10.3847/2041-8213/abec78 doi: 10.3847/2041-8213/abec78

Urbář, J., Němeček, Z., Šafránková, J., & Přech, L. (2019). Solar wind proton deceleration in front of the terrestrial bow shock. *Journal of Geophysical Research: Space Physics*, *124*(8), 6553-6565. Retrieved from https://agupubs.onlinelibrary.wiley.com/doi/abs/10.1029/2019JA026734 doi: https://doi.org/10.1029/2019JA026734